Article

Numerical approach determining the optimal distance separating two heat sources heated by joule effect in a square cavity

Mohammed Salah Belalem[1,*], Abdelkader Ferhah[1], Toufik Chergui[2]

[1] Energetics in Arid Zones Laboratory ENERGARID Laboratory, Bechar University, Bechar 08-000, Algeria

[2] Renewable Energy Applied Research Unit, URAER, CDER, Ghardaïa 47-133, Algeria

* Corresponding author: Mohammed Salah Belalem, belalemmedsalah@yahoo.com

Abstract: This study presents a comprehensive two-dimensional numerical analysis of natural laminar convection within a square cavity containing two circular heat sources, which simulate electric cables generating heat due to Joule heating. This scenario is particularly relevant in aeronautics, where excessive heating of electrical installations can lead to significant material and human safety risks. The primary objective of this research is to identify the optimal spacing between the two heat sources to mitigate the risk of overheating and ensure the safe operation of the electrical installation. To achieve this, various configurations were analyzed by adjusting the distance between the heat sources while also varying the Rayleigh number across a range from 10^3 to 10^6. The governing equations for the fluid flow and heat transfer were solved using a FORTRAN-based numerical code employing the finite volume method. The results indicate that the heat transfer characteristics within the cavity are significantly influenced by both the distance between the heat sources and the Rayleigh number. The analysis revealed that the average Nusselt number (Nu_{avg}) peaked at a value of 14.69 when the distance between the heat sources was set at 0.7 units and the Rayleigh number was at 10^6. This finding suggests that maintaining this specific spacing between the electrical cables can optimize heat dissipation and enhance the safety of the installation. In conclusion, the study recommends adopting a spacing of 0.7 units between the electrical cables to ensure optimal thermal performance and minimize the risk of overheating, thereby safeguarding both the materials and personnel involved in aeronautical operations.

Keywords: natural convection; heat source; optimal distance; finite volume; joule effect; electrical installation

1. Introduction

The importance of this work lies in the vast use of relatively simple form obstacles, square, for example in industrial applications. Many scientific works have been published to analyze the phenomenon of cooling electronic and/or electrical components using convection in its three forms. Among these published works, we quote:

Ortega and Moffat [1] performed natural convection experiments on cooling blocks simulating electronic components. The blocks are mounted on one of two parallel and vertical walls (80 blocks arranged in an arrangement of 8 columns and 10 rows).

Patnana et al. [2] numerically simulated the incompressible flows of non-Newtonian fluids around a circular cylinder in an unsteady regime, the work was established with the commercial code (Fluent), and the Reynolds number varies between $40 \leq Re \leq 140$, the power index $0.4 \leq n \leq 1.8$, the Prandtl number $1 \leq Pr \leq$

100. The results show that thinning fluids enhance the increase in heat transfer against obstacle-thickening fluids. Also, the increase in the fluid power index generates many more vortices, on the other hand, the size of the vortices decreases with the increase in the Reynolds number.

Chandra and Chhabra [3] carried out a numerical simulation study of the incompressible flow around a semi-circular and unconfined cylinder. The study touches on the hydrodynamic and thermal spirit. They determined values called Reynolds numbers, critical for the appearance of vortices behind the obstacle. In conclusion, this study suggests the evolution of the drag coefficient with respect to the variation of Reynolds numbers.

Kumar and Dhiman [4] conducted a numerical study for Reynolds numbers $1 \leq Re \leq 100$, Richardson $0 \leq Ri \leq 1$, and blocking rates $10\% \leq \beta \leq 50\%$, the mixed convection of a heated cylinder square arranged in a vertical channel. Air was taken as the driving fluid. The authors observed a transition from a stable flow regime to a periodic flow regime at different Richardson numbers (Ri) and Reynolds numbers (Re), (for a Ri = 0, at Re = 35, 65, 74 and 62), (Ri = −0.5, at Re = 12, 39, 48 and 54), and (Ri = −1, at Re = 9, 30, 39 and 50) for a blocking ratio β = 10%, 25%, 30% and 50%, respectively. The onset of the flow separation is also determined. Finally, the authors determined correlations for the Strouhal number, for the drag coefficient, and for the heat transfer coefficient. Laidoudi and Bouzit [5] conducted a numerical study using the commercial code ANSYS CFX to examine the effects of thermal buoyancy on the thermohydrodynamic characteristics of an incompressible Poiseuille flow around symmetrically confined and asymmetrically immersed cylinders. Numerical results were presented and discussed for the following condition ranges: $10 \leq Re \leq 40$, Richardson number $0 \leq Ri \leq 4$, and the eccentricity factor $0 \leq \varepsilon \leq 0.7$ for a Prandtl number Pr = 1 and a blocking rate B = 20%.

Amieur and Amieur [6] investigate the complex interactions between fluid flow and thermal dynamics when a laminar flow encounters a fixed obstacle. Using the finite element method (FEM), the research focuses on how various geometric parameters of the obstacle, specifically its height and shape (rectangular, triangular, or half-cylindrical) affect the thermo-hydrodynamic behavior of the flow. The results indicate that the flow structure is significantly influenced by the size and shape of the turbulator. Specifically, the presence of vortex structures both upstream and downstream of the turbulator can be attributed to two main factors: the presence of a heat source and the pressure drops caused by the obstruction of the flow. These pressure drops are primarily determined by the geometric parameters of the turbulator, which affect how the fluid interacts with the obstacles. This interaction leads to complex flow patterns that can enhance mixing and heat transfer in various applications.

Chiocca et al. [7] used the finite element method to evaluate the ability of different thermal methods used to simulate a gas metal arc welding process pass to reproduce the temperature distribution around the weld, which was low; the results obtained are compared to experimental measurements. The study showed that in the vicinity of the weld bead, very similar thermal behaviors can be obtained with each of the methods analyzed. A very good agreement was found when comparing the experimental measurements with the numerical simulations.

To estimate heat transfer in low-pressure cavities, Alkhalidi et al. [8] used the finite volume method to solve the governing equations as well as the temperature jump and slip flow boundary conditions for different cavity aspect ratios (H/L) and Rayleigh numbers for macro and microfluids. The results show that the heat transfer ratios become significant when the Rayleigh number is high and when the aspect ratio is less than 5.

Lan and Jiao [9] numerically simulated the quasi-critical natural convection of water in a cylindrical hydrothermal reactor. The results show that natural convection is dominated by a large high-speed vortex when the heat flux ratio is less than 1, and it is dominated by two independent weak vortices when the heat flux ratio is greater than 1. When the temperature approaches the pseudocritical. At this point, the flow structure remains qualitatively unchanged, but wall heat transfer is enhanced and fluid motion is generally weakened. The study, design, and development of algorithmic solutions for the detection of thermal peaks in the case of multiple heat sources (number of heat sources greater than "one") have been carried out.

Fathi [10] used the methodology of the GDSCAN algorithm (which is a thermal scanning algorithm based on GDS (Gradient Detection Sensor) for multiple detection of heat sources in integrated circuits). The GDSCAN algorithm provided highly accurate temperature estimates with an error margin of no more than 1.5% and an optimal sensor network architecture including minimal thermal sensors.

Faraji et al. [11] considered the natural convection caused by melting in an inclined rectangular enclosure filled with a nano-enhanced phase change material, analyzing the effect of the insertion of nanoparticles by quantifying their contribution to the transfer of global heat. The case is heated from below using a protruding heat source (microprocessor) generating heat at a constant and uniform volumetric flow rate and mounted on a substrate (motherboard). All walls are considered adiabatic. The results obtained show that the insertion of nanoparticles has a significant quantitative effect on the overall heat transfer. They also show that the insertion of metal nanoparticles of different concentrations affects the thermal behavior of the heat sink, which contributes to the efficient cooling of the heat source.

In an analysis, Hussain et al. [12] explored the stagnation point of the Jeffery liquid flow on an expandable cylinder. The Cattaneo-Christov model with double stratification, heat source and thermal relaxation was used to study heat and mass transfer. The results of the study show that higher values of the ratio parameter reduce the magnitude of the drag coefficient, while an opposite trend is noted for a higher Deborah number in terms of delay time and curvature of the drag parameter.

Vinodkumar Reddy et al. [13] carried out an exploration study of the convective flow of the MHD stagnation point of Casson nanofluid on a stretching sheet in a porous medium with higher order chemical reactions and multiple slips. Thermal transmission was examined in the presence of radiation, Joule heating, viscous dissipation and heat source. The results show that increasing the values of Joule radiation and heating parameters, as well as the Eckert number, leads to an increase in temperature.

Benouis Fatima Zohra [14] Improving the cooling of electronic components in critical environments was considered through detailed simulations. The results provided that the introduction of fins into the cooling system allows a significant improvement in heat transfer, thus contributing to better dissipation of heat generated

by electronic components. Additionally, the analyses revealed that a few fin configurations, such as flat plate fins and pin fins, offer distinct advantages in terms of cooling efficiency and power consumption. Flat plate fins have been shown to be effective in optimizing heat transfer under certain conditions, while pin fins have demonstrated the ability to reduce energy consumption due to their innovative design. Paving the way for more efficient and durable cooling solutions for electronic components in modern IT environments.

Our work aims to study natural laminar convection in a square cavity containing two circular heat sources heated by the Joule effect and modeling two electrical cables. The discoveries may affect several sectors and applications, in particular the aeronautical sector (subject of the study), industrial and domestic electrical installations. The main objective will therefore be to find the optimal distance between the heat sources and which must be respected to avoid excessive heating which could damage the installation and cause material and human damage.

2. Materials and methods

2.1. Physical model and boundary conditions

The physical model studied (see **Figure 1**) is a square cavity with isothermal side walls H, containing two heat sources of circular shape and diameter D = 0.1H, the distance between the sources is to model two electrical cables in which passes an electric current producing a release of heat by the Joule effect (**Table 1**).
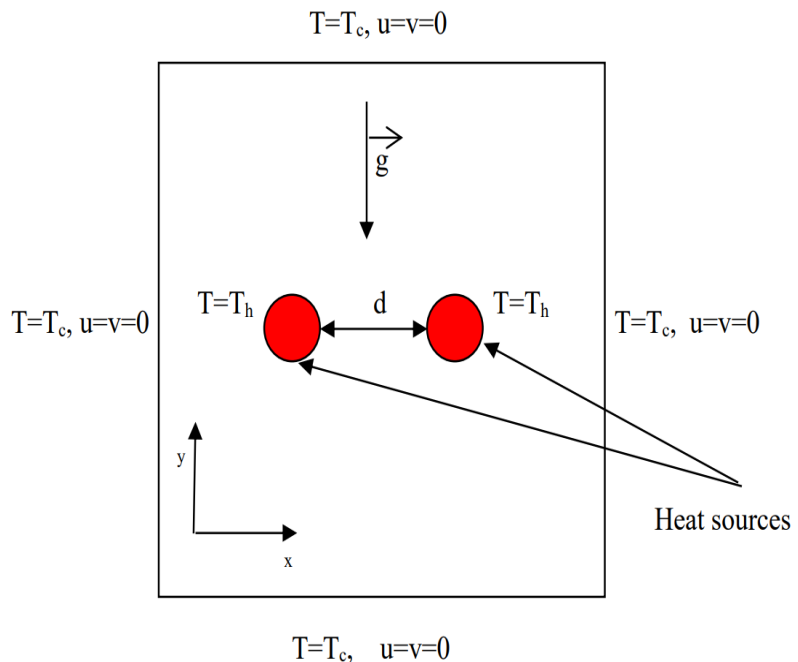
Figure 1. Physical model.

Table 1. Boundary conditions.

Wall	Speed	Temperature
All walls	$u = v = 0$	$T = T_c$

The aim is to determine the optimum distance between the two heat sources to avoid excessive heating of the installation. For this we vary the dimensionless distance between the sources $d = 0.4H$, $0.5H$, $0.6H$ and $0.7H$ and this for different values of the Rayleigh number $Ra = 10^3$, 10^4, 10^5, 10^6.

2.2. Mathematical formulation

To establish a simple mathematical model for the physical problem, we made assumptions to facilitate its solution, namely:

- The fluid is Newtonian and incompressible.
- The medium is continuous.
- The flow is two-dimensional.
- The diet is laminar.
- The viscous dissipation is negligible ($\mu_\Phi = 0$).
- The Boussinesq approximation is validated everywhere.
- The cables are not insulated.
- The magnetic field is negligible

Equation of continuity

$$\left(\frac{\partial u}{\partial x} + \frac{\partial v}{\partial y}\right) = 0 \tag{1}$$

Momentum equation along the *x* axis

$$\rho\left(u\frac{\partial u}{\partial x} + v\frac{\partial u}{\partial y}\right) = -\frac{\partial p}{\partial x} + \mu\left[\frac{\partial^2 u}{\partial x^2} + \frac{\partial^2 u}{\partial y^2}\right] \tag{2}$$

Momentum equation along the y axis

$$\rho\left(u\frac{\partial v}{\partial x} + v\frac{\partial v}{\partial y}\right) = -\frac{\partial p}{\partial y} + \mu\left[\frac{\partial^2 v}{\partial x^2} + \frac{\partial^2 v}{\partial y^2}\right] + g\beta(T - T_0) \tag{3}$$

Energy equation

$$u\frac{\partial T}{\partial x} + v\frac{\partial T}{\partial y} = \frac{\lambda}{\rho C_P}\left[\frac{\partial^2 T}{\partial x^2} + \frac{\partial^2 T}{\partial y^2}\right] \tag{4}$$

2.2.1. Dimensional equations

The dimensionless form is used to find general solutions to physical problems independently of measurement systems. It also simplifies the resolution of equation systems and reduces physical parameters. To display the control parameters of the problem studied, it is necessary to introduce reference quantities.

Reference quantities:

$$x^* = \frac{x}{L_{\text{ref}}}, y^* = \frac{y}{L_{\text{ref}}}, t^* = \frac{tV_r}{L_{\text{ref}}}, u^* = \frac{u}{V_{\text{ref}}},$$

$$v^* = \frac{v}{V_{\text{ref}}}, p^* = \frac{p}{\rho V_{\text{ref}}^2}, T^* = \frac{T - T_\infty}{\Delta T}, t^* = \frac{t}{t_{\text{ref}}},$$

with: $u_{\text{ref}} = \sqrt{g\beta\Delta\text{TH}}$: reference speed, $T_{\text{ref}} = \frac{Th-Tc}{2}$: reference temperature, $p_{\text{ref}} = \rho u^2$: reference pressure, $t_{\text{ref}} = \frac{H}{\sqrt{g\beta\Delta\text{TH}}}$: reference time

2.2.2. Dimensionless equations

Equation of continuity

$$\frac{\partial(u^*)}{\partial x^*} + \frac{\partial(v^*)}{\partial y^*} = 0 \tag{5}$$

Momentum equation along the *x* axis

$$u^* \frac{\partial u^*}{\partial x^*} + v^* \frac{\partial u^*}{\partial y^*} = -\frac{\partial p*}{\partial x^*} + \sqrt{\frac{\text{Pr}}{\text{Ra}}}\left[\frac{\partial^2 u^*}{\partial x^{*2}} + \frac{\partial^2 u^*}{\partial y^{*2}}\right] \tag{6}$$

Momentum equation along the *y* axis

$$u^* \frac{\partial v^*}{\partial x^*} + v^* \frac{\partial v^*}{\partial y^*} = -\frac{\partial p*}{\partial y^*} + \sqrt{\frac{\text{Pr}}{\text{Ra}}}\left[\frac{\partial^2 v^*}{\partial x^{*2}} + \frac{\partial^2 v^*}{\partial y^{*2}}\right] + \text{Pr}.\text{Ra}.\Delta\text{T} \tag{7}$$

Energy equation

$$u^* \frac{\partial T^*}{\partial x^*} + v^* \frac{\partial T^*}{\partial y^*} = \frac{1}{\sqrt{\text{Pr}.\text{Ra}}}\left[\frac{\partial^2 T^*}{\partial x^{*2}} + \frac{\partial^2 T^*}{\partial y^{*2}}\right] \tag{8}$$

With: $\text{Pr} = c_p\mu/\lambda_f$ Prandtl number, $\text{Ra} = \rho g\beta\Delta\text{TH}^3/\mu^2$ Rayleigh number, $\Delta\text{T} = T_h - T_c$: difference between hot and cold temperature.

3. Results and discussion

3.1. Hydrodynamic field

The **Figure 2a,b,e,f**, **Figure 3a,b,e,f**, **Figure 4a,b,e,f**, and **Figure 5a,b,e,f** show the appearance of the streamlines as a function of the variation of the distance between heat sources and the variation of the Rayleigh number. From the **Figure 5a,b,e,f** which shows the evolution of the stream lines as a function of the Rayleigh number for a distance between heat sources *d* = 0.7, the flow field remain symmetrical with respect to the vertical axis of the cavity for any Rayleigh value. It can be seen that for Ra = 10^6, our flow field is essentially formed by four main cells of opposite direction two by two at the top of the cavity thus favoring the convective heat transfer in the cavity. **Figure 2a,b,e,f** shows the evolution of the streamlines as a function of the Rayleigh number for *d* = 0.4 our flow field is symmetrical with respect to the diagonal of the cavity. Notice for Ra = 10^5 that the flow field starts to lose its symmetry, with the cell rise from bottom right upward, giving rise to two small fluid recirculation cells near the right source with vortex formation at the upper corner of the cavity.

Figure 2. (**a**) Streamlines; (**c**) isotherms, Ra = 10^3; (**b**) Streamlines; (**d**) isotherms, Ra = 10^4; (**e**) Streamlines (**g**) isotherms, Ra = 10^5; (**f**) Streamlines; (**h**) isotherms, Ra = 10^6 (d = 0.4).
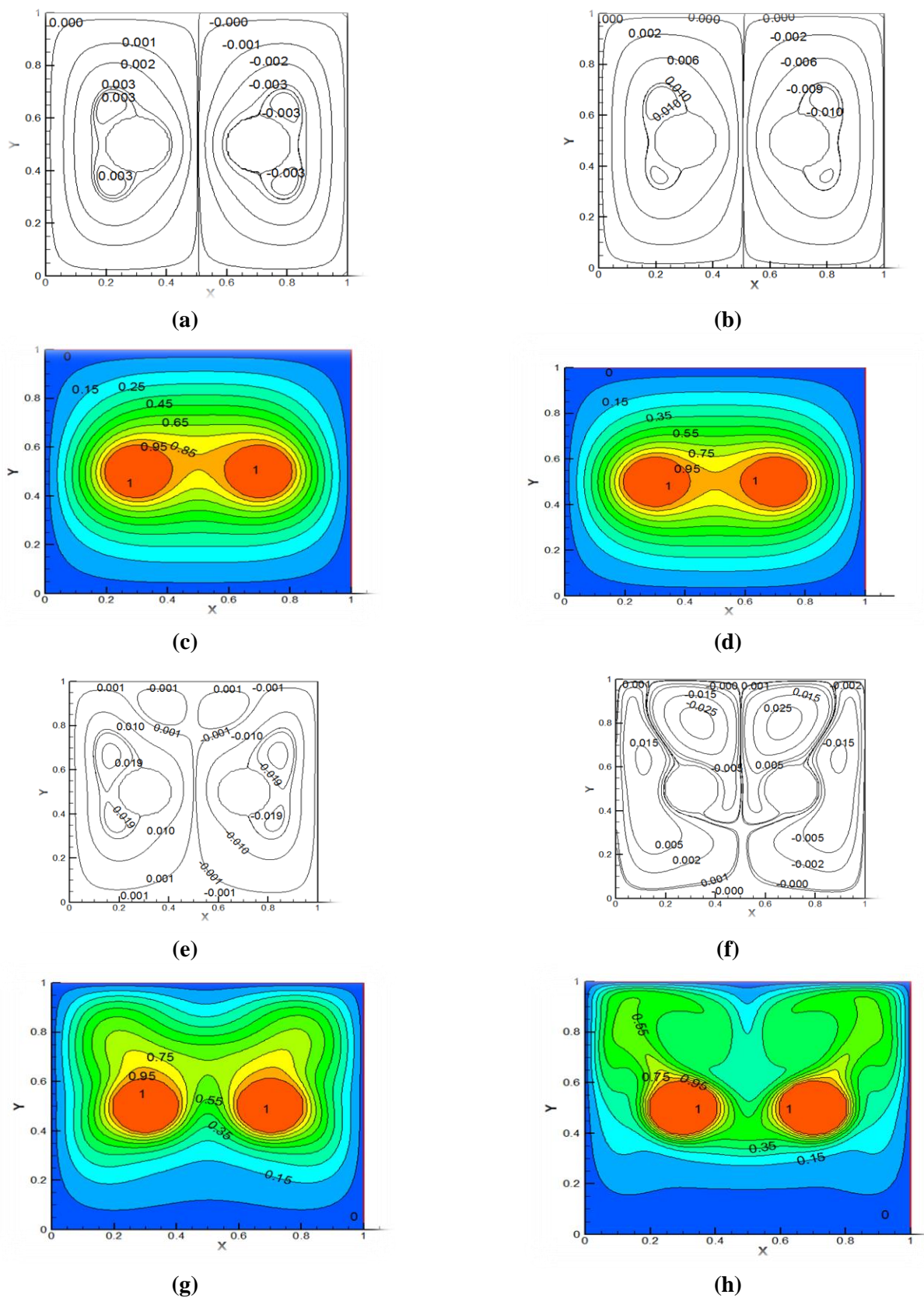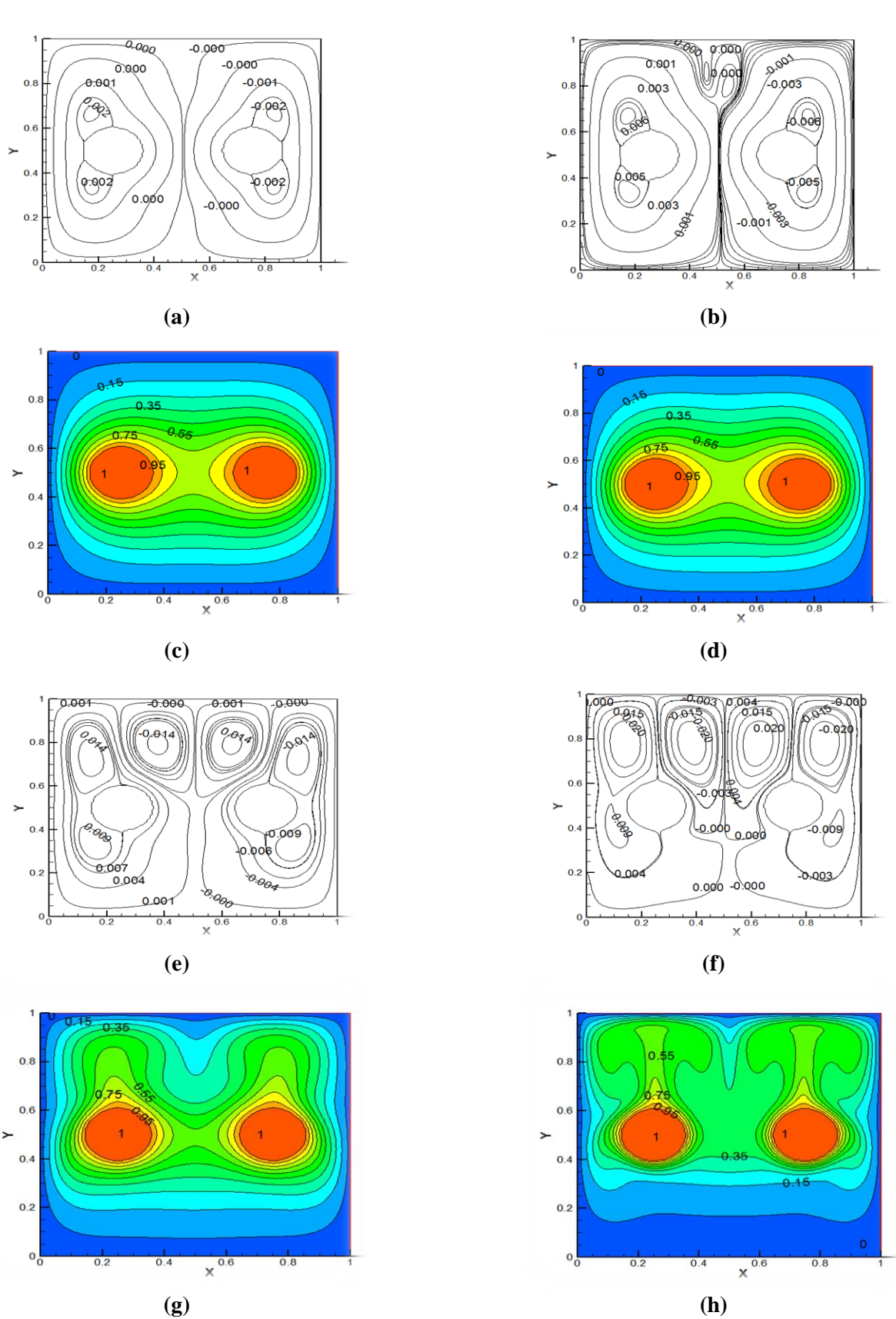
Figure 3. (**a**) Streamlines; (**c**) isotherms, Ra = 10^3; (**b**) Streamlines; (**d**) isotherms, Ra = 10^4; (**e**) Streamlines (**g**) isotherms, Ra = 10^5; (**f**) Streamlines; (**h**) isotherms, Ra = 10^6; (d = 0.5).
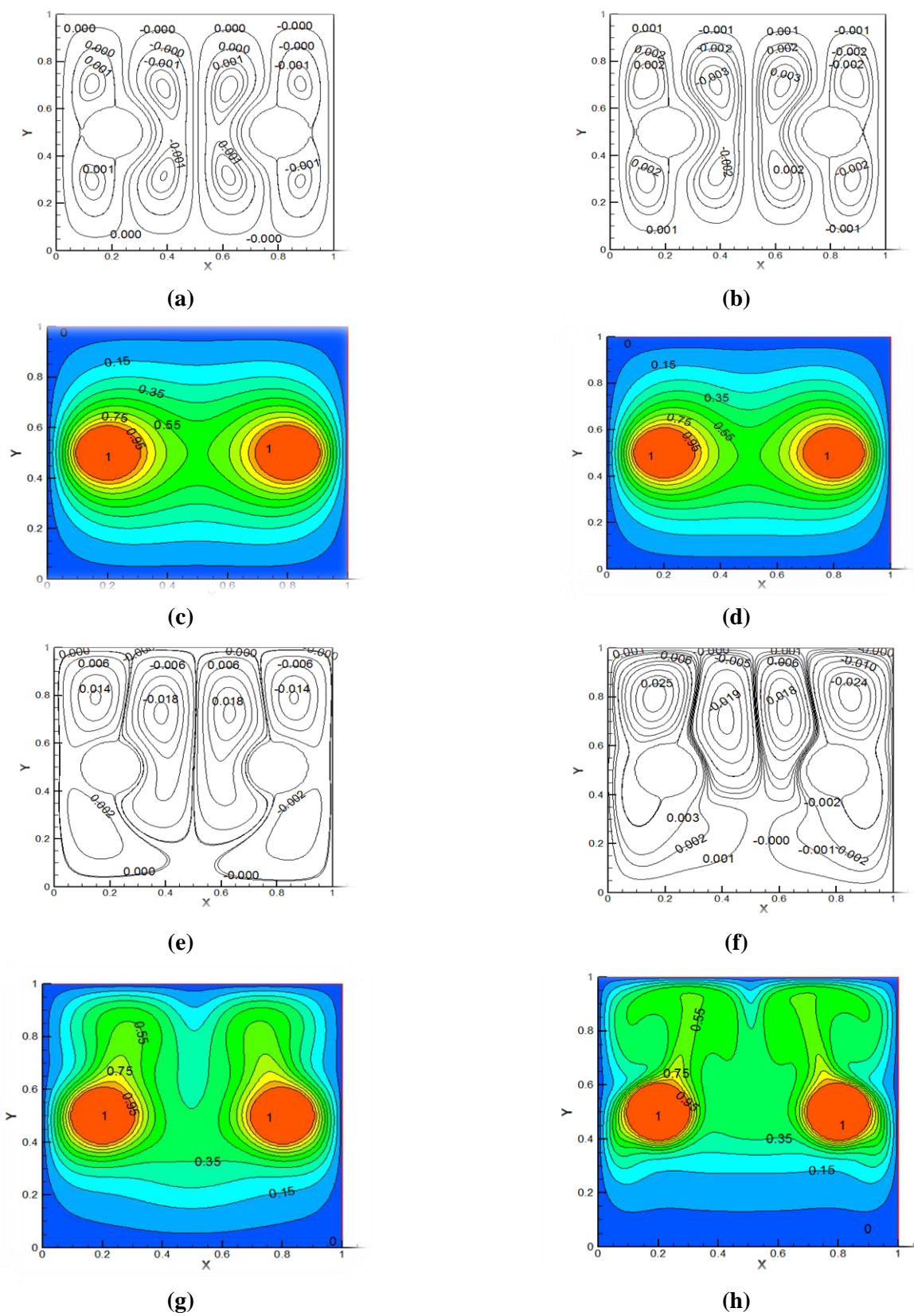
Figure 4. (**a**) Streamlines; (**c**) isotherms, Ra = 10^3; (**b**) Streamlines; (**d**) isotherms, Ra = 10^4; (**e**) Streamlines (**g**) isotherms, Ra = 10^5; (**f**) Streamlines; (**h**) isotherms, Ra = 10^6; (*d* = 0.6).
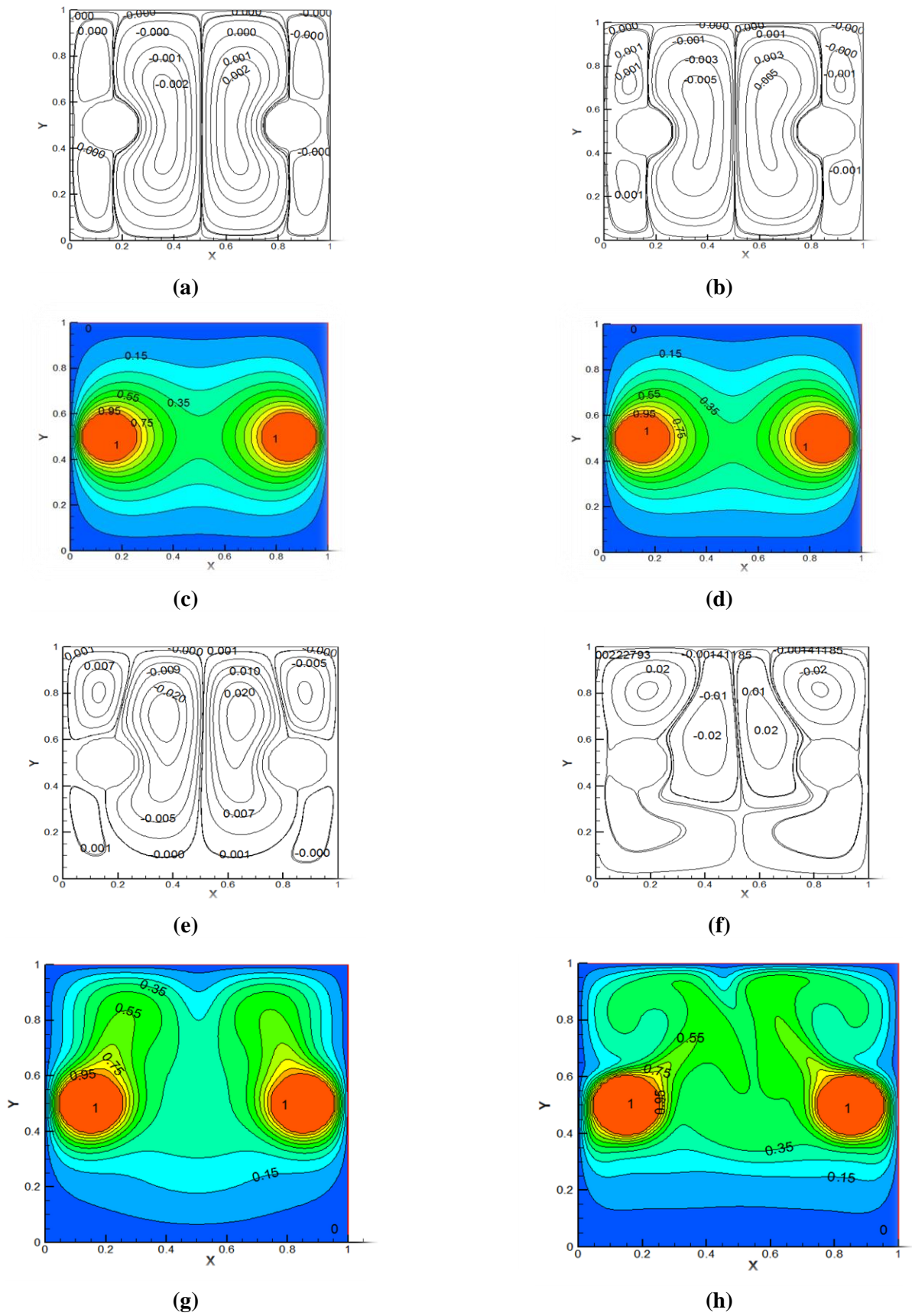
Figure 5. (**a**) Streamlines; (**c**) isotherms, Ra = 10^3; (**b**) Streamlines; (**d**) isotherms, Ra = 10^4; (**e**) Streamlines (**g**) isotherms, Ra = 10^5; (**f**) Streamlines; (**h**) isotherms, Ra = 10^6; (d = 0.7).

3.2. Thermal field

From **Figure 5c,d,g,h**, which shows the contours of the isotherms for a distance separating the two heat sources equal to 0.7, it can be seen that for a Rayleigh value equal to 106 that the hottest zone is located around the sources of heat. Air recirculation results in the formation of the high-temperature zones of curvilinear shape which is oriented towards the upper corners and the central part above the two sources. It is also observed that the entire area below the two heat sources is a cold or "dead" zone. It is therefore a question of an acceleration of the natural convection mechanism. The lightest layers, i.e., the least dense ones, the warmer ones are dragged upwards due to the force of gravity. These same layers cool along the walls of the enclosure which is colder than the heat sources.

Influence of the rayleigh number (Ra)

a) d = 0.4, 0.5

The **Figure 2c,d,g,h**, **Figure 3c,d,g,h**, **Figure 4c,d,g,h**, and **Figure 5c,d,g,h** shows the appearance of the isotherms as a function of the variation of the distance heat sources and the Rayleigh number. which show the contours of the isotherms for a distance separating the two heat sources equal to 0.4 and 0.5 respectively in horizontal position and for different Rayleigh values, we see that for Ra = 10^3 and Ra = 10^4 the isotherm lines are tight in the vicinity of the two sources and they move away from the walls of the cavity and this is essentially due to the fact that the highest temperatures are find heat sources nearby, which indicates the heat exchange in the cavity is in a conductive state. For Rayleigh values equal to 10^5 and 10^6 we see that the hottest zone is located around the heat sources. Air recirculations result in the formation of a high temperature zone with a curvilinear shape. We also observe that the entire area located below the two heat sources is a cold or "dead" zone. This is indeed the mechanism of natural convection. The lightest layers, i.e., the least dense, i.e., the warmest, are pulled upwards due to the force of gravity. These same layers cool along the walls of the enclosure which is lower than that of the sources, that is to say colder. As they cool, they become heavier, but they still remain a little lighter than the lower layers located below the sources which remain cold.

b) d = 0.6, 0.7

According to **Figure 4c,d,g,h** and **Figure 5c,d,g,h** which show the contours of the isotherms for a distance separating the two heat sources equal to 0.6, and 0.7 respectively in horizontal position and for different values of Rayleigh we can see that for Ra = 10^3 and Ra = 10^4 the same phenomenon as for the previous cases (d = 0.4 and 0.5). For Rayleigh values equal to 10^5 and 10^6 we see that the hottest zone is located around the heat sources. The air recirculations lead to the formation of high-temperature zones with a curvilinear shape which is oriented towards the upper corners and the central part above the two sources. We also observe that the entire area located below the two heat sources is a cold or "dead" zone. It is therefore an acceleration of the natural convection mechanism. The lightest layers, i.e., the least dense, i.e., the warmest, are pulled upwards due to the force of gravity. These same layers cool along the walls of the enclosure which is lower than that of the sources, that is to say colder. As they cool, they become heavier, but they still remain a little lighter than the lower layers located below the sources which remain cold.

4. Maximum stream function (ψ_{max})

Which describes the movement of particles according to their displacement, speed and acceleration without taking into consideration the original forces of this movement. The stream function (ψ) is calculated as follows:

$$u = \frac{\partial \psi}{\partial y} \; et \; v = -\frac{\partial \psi}{\partial x}.$$

Figure 6 illustrates the appearance of the maximum stream function as a function of the variation of the distance and the Rayleigh number. According to this figure we notice that for values of Ra between 10^3 and 10^4 the stream function takes a small and almost constant maximum value regardless of the distance between the heat sources, which indicates that the heat transfer in the cavity is more conductive than convective. While for Rayleigh greater than 10^5 and especially for the value of 10^6, Ψ_{max} takes its maximum value for a distance separating the sources equal to 0.7. We conclude that the heat transfer rate in this case is maximum.
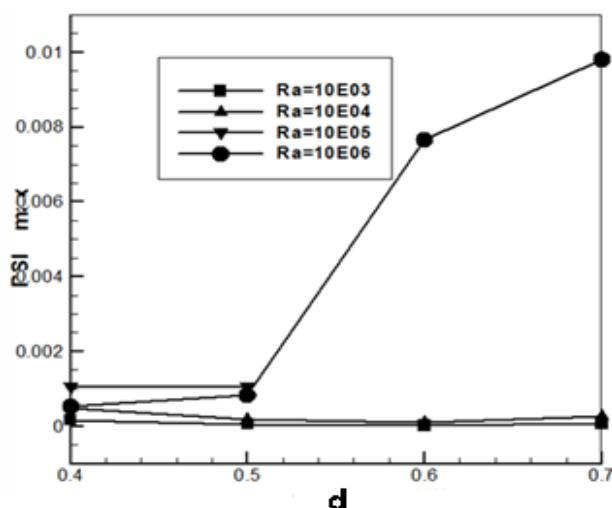
Figure 6. Variation of maximum stream function (Ψ_{max}) for different values of the distance between heat sources.

So, for low values of the Rayleigh number, we can conclude that the heat transfer to the cavity is ensured by conduction, something which does not favor the cooling of the heat sources (cables) and therefore can create a risk for our installation and consequently material and human damage. For values of the Rayleigh number greater than 10^4 and more particularly values 10^5 and 10^6, we see that the heat transfer is convective, this facilitates the flow of hot air surrounding the heat sources and consequently cools the internal environment of the cavity which avoids all risks that could damage our installation.

5. Heat transfer rate

The rate of heat transfer by convection in an enclosure is obtained from the calculation of the Nusselt number, which is a dimensionless number, it represents the ratio between the heat flow exchanged by convection to that by conduction. It is

defined as follows: $Nu = \frac{hL}{\lambda}$, with:

  h: heat transfer coefficient (W·m^{-2}·K^{-1})

  L: characteristic length (m)

  λ: thermal conductivity (W·m^{-1}·K^{-1})

  The average Nusselt number is defined as:

$$\overline{Nu} = \frac{1}{L}\int_0^L Nu\,dx.$$

5.1. Influence of the distance between heat sources (d)
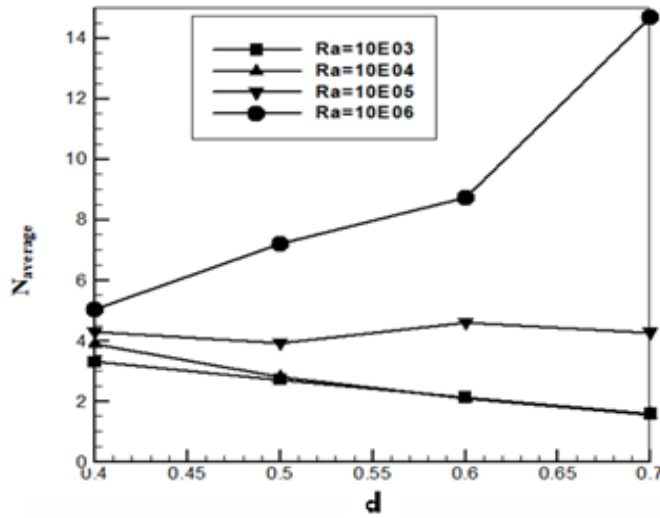
Figure 7. Variation of average nusselt number (Nu$_{Avg}$) for different values of the distance between heat sources.

According to the **Figure 7**, which shows the evolution of the average Nusselt number as a function of the distance between the sources in the case where the two sources are, we see that for values of $d = 0.4$ and $d = 0.6$, there is a slight increase in the average Nusselt number by increasing the Rayleigh number (from 10^3 to 10^6), this means that the heat transfer improves slightly by moving the sources away from each other and by increasing the Rayleigh value. For $d = 0.7$ we notice that the average Nusselt number reaches a maximum value for Ra $= 10^6$, which implies that convection is favored in this case.

5.2. Influence of the rayleigh number (Ra)

From the **Figure 8**, which shows the evolution of the average Nusselt number as a function of the Rayleigh number for each position of the two sources, we see that for Rayleigh values lower than 10^5, there is a slight decrease in the latter by increasing the distance between the sources (from 0.4 to 0.7), which implies that the heat transfer is not affected by these Rayleigh values. From Ra $= 10^6$ we notice a clear increase in average Nusselt as a function of the distance between the two heat sources which is favored by the increase in Ra.
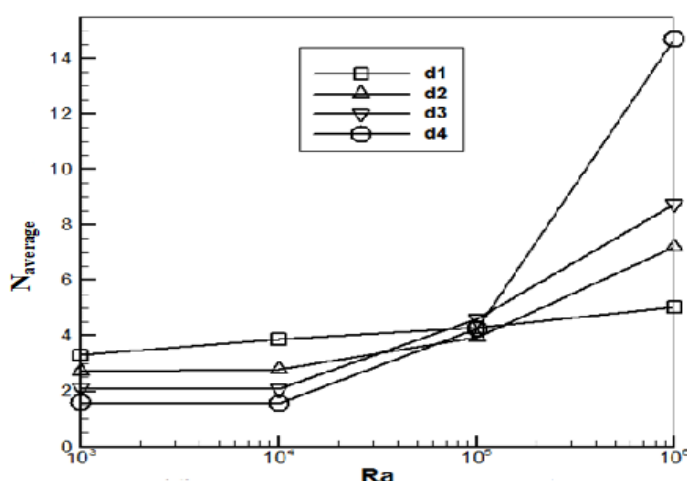
Figure 8. Variation of average nusselt number (Nu_{Avg}) versus different values of rayleigh number (Ra).

5.3. Average nusselt number (Nu_{avg})

From the **Figure 8**, which shows us the evolution of the average Nusselt number as a function of the position of the heat sources for values of the Rayleigh number from 10^3 and 10^6, we notice that the average Nusselt value increases as a function of the distance between the two heat sources, which means that the heat transfer in the cavity improves by increasing the distance between the sources, we can see that the average Nusselt number increases slightly for all distances between the two heat sources for the number Rayleigh values included between 10^3 and 10^4, this is completely normal since the heat transfer between the sources of heat and the ambient environment is mainly by conduction, we observe a clear evolution of the average Nusselt number for the values of the Rayleigh number beyond 10^4.

In the case for Ra = 10^5 and according to the **Figure 8**, we see that whatever the distance between the two heat sources, the Nusselt number takes the same value, that is to say that the heat transfer in the cavity is not influenced by the spacing between the two heat sources for this value of the Rayleigh number. For Ra = 10^6, in this case, a first observation to make is that for the distance separating the two heat sources heat equal to 0.7 the convective heat transfer in the cavity is favored by the strong air circulation due essentially to the increase in the Rayleigh number. We also notice that the average Nusselt value increases as a function of the distance between the two heat sources, which means that the heat transfer in the cavity improves by increasing the distance between the sources.

6. Conclusion

The study presented concerns the numerical simulation of two-dimensional natural convection in laminar regime, in a square cavity with isothermal walls. The cavity in question contains two circular heat sources, simulating two electric cables through which an electric current passes which produces heat release by the Joule effect.

The main objective of this work was the search for the optimal distance between the heat sources, which allows a maximum heat transfer to avoid excessive heat generation in the cavity. The finite volume method was used to discretize the equations governing our steady-state convection flow in steady state, and the SIMPLE algorithm was used to solve them. The results obtained show that the heat transfer in the cavity is affected mainly by the spacing between the two heat sources and the variation of the Rayleigh number (**Figure 6**). Indeed, for the position of heat sources in the cavity, we note the heat transfer in the cavity is maximum ($Nu_{Avg} = 14.69$), for a distance between the heat sources equal to 0.7 and a value of Rayleigh 10^6 (**Figure 7**).

In conclusion, we can say that the optimum distance between the two sources of heat and which has been the subject of this study is reached in the case where the distance between sources is equal to 0.7, which is the optimal distance that can keep our installation safe and far from any risk caused by joule effect.

Author contributions: Conceptualization, MSB and TC; methodology, MSB; software, AF; validation, MSB, TC and AF; formal analysis, MSB and AF; investigation, MSB; resources, MSB; data curation, MSB; writing—original draft preparation, MSB; writing—review and editing, MSB; visualization, MSB and TC; supervision, TC; project administration, MSB and AF; funding acquisition, MSB and AF. All authors have read and agreed to the published version of the manuscript.

Conflict of interest: The authors declare no conflict of interest.

References

1. Ortega A, Moffat RJ. Buoyancy induced convection in a non-uniformly heated array of cubic elements on a vertical channel wall. Stanford University; 1986.
2. Patnana VK, Bharti RP, Chhabra RP. Two-dimensional unsteady forced convection heat transfer in power-law fluids from a cylinder. International Journal of Heat and Mass Transfer. 2010; 53(19–20): 4152–4167. doi: 10.1016/j.ijheatmasstransfer.2010.05.038
3. Chandra A, Chhabra RP. Flow over and forced convection heat transfer in Newtonian fluids from a semi-circular cylinder. International Journal of Heat and Mass Transfer. 2011; 54(1–3): 225–241. doi: 10.1016/j.ijheatmasstransfer.2010.09.048
4. Kumar D, Dhiman A. Opposing buoyancy characteristics of Newtonian fluid flow around a confined square cylinder at low and moderate Reynolds numbers. Numerical Heat Transfer, Part A: Applications. 2016; 69(8): 874–897. doi: 10.1080/10407782.2015.1090838
5. Laidoudi H, Bouzit M. Mixed convection in poiseuille fluid from an asymmetrically confined heated circular cylinder. Thermal Science. 2018; 22(2): 821–834. doi: 10.2298/tsci160424172l
6. Amieur R, Amieur A. Contribution to the COMSOL simulation of the effector hydrodynamics of the presence of a turbulator in a flow [Master's thesis]. University of Ghardaia, Algeria; 2018.
7. Chiocca A, Frendo F, Bertini L. Evaluation of Heat Sources for the Simulation of the Temperature Distribution in Gas Metal Arc Welded Joints. Metals. 2019; 9(11): 1142. doi: 10.3390/met9111142
8. Alkhalidi A, Kiwan S, Al-Kouz W, et al. Rarefaction and scale effects on heat transfer characteristics for enclosed rectangular cavities heated from below. Thermal Science. 2019; 23(3 Part B): 1791–1800. doi: 10.2298/tsci170621234a
9. Lan S, Jiao F. Modeling of heat source in grinding zone and numerical simulation for grinding temperature field. Int J Adv Manuf Technol. 2019; 103: 3077–3086. doi: 10.1007/s00170-019-03662-w
10. Fathi BH. Study, design and development of a thermal peak detection algorithm for multiple heat sources in integrated circuits (French) [PhD Theis]. Université du Québec en Outaouais; 2019. p. 111.
11. Faraji M, Faraji H, El Alami M. Numerical simulation of the cooling of an electronic component: effect of the angle of inclination (French). In: Proceedings of the 28ème Congrès Français de Thermique; 2020.

12. Hussain Z, Hussain A, Anwar MS, et al. Analysis of Cattaneo–Christov heat flux in Jeffery fluid flow with heat source over a stretching cylinder. J Therm Anal Calorim. 2022; 147: 3391–3402. doi: 10.1007/s10973-021-10573-0

13. Vinodkumar Reddy M, Vajravelu K, Lakshminarayana P, Sucharitha G. Heat source and Joule heating effects on convective MHD stagnation point flow of Casson nanofluid through a porous medium with chemical reaction. Numerical Heat Transfer, Part B: Fundamentals. 2023; 85(3): 286–304. doi:10.1080/10407790

14. Benouis F. Z. Cooling analysis of heat sources placed in a ventilated cavity - application to data centers [PhD thesis]. Usthb University; 2024.